Materials Express

2158-5849/2014/4/508/013
doi:10.1166/mex.2014.1201
www.aspbs.com/mex

Article

Linear and nonlinear optical susceptibilities of bilayer graphene

Ali H. Reshak[1,2,*] and Sushil Auluck[3]

[1]*New Technologies – Research Center, University of West Bohemia, Univerzitni 8, 306 14 Pilsen, Czech Republic*
[2]*Center of Excellence Geopolymer and Green Technology, School of Material Engineering, University Malaysia Perlis, 01007 Kangar, Perlis, Malaysia*
[3]*Council of Scientific and Industrial Research – National Physical Laboratory Dr. K S Krishnan Marg, New Delhi 110012, India*

ABSTRACT

The linear and nonlinear optical susceptibilities of bilayer pristine graphene (BLPG) and H_2S single molecule adsorbed at three different sites on a single graphene sheet of BLPG are calculated to obtain further insight into the electronic properties. Calculations show that the adsorption of H_2S on the bridge and top sites open a gap around the Fermi level, while adsorption of H_2S on the hollow site closes the energy gap, resulting in significant changes in the linear and nonlinear optical susceptibilities. This is attributed to the fact that the adsorbed H_2S onto a single graphene sheet of BLPG cause significant changes in the electronic structure. The calculated linear optical susceptibilities show a huge anisotropy confirming that the graphene has unusual and interesting optical properties. We find that the absorption spectrum of graphene is quite flat extending from 300–2500 nm with an absorption peak in the UV region (~270 nm), which is in excellent agreement with the experimental data. The pristine graphene shows a strong saturable absorption because of a large absorption and Pauli blocking. We have calculated the nonlinear optical susceptibilities of BLPG and the three configurations and found that they possess a huge second harmonic generation. We have also calculated the microscopic hyperpolarizability, β_{ijk}, for BLPG.

Keywords: Bilayer Pristine Graphene, Graphene Sheet, H_2S, Linear and Nonlinear Optical Susceptibilities, DFT.

1. INTRODUCTION

Because of its exceptional physical properties, graphene has attracted the attention of many research workers. The outstanding mechanical,[1] electrical[2] and physical properties[3] of graphene warrants its use in a variety of areas such as hydrogen technology,[4] electronics,[2] sensing[5] and drug delivery,[6,7] among many others. Graphene is a honeycomb two dimensional lattice of a monolayer of carbon atoms.[8,9] Graphene consists of a single atomic layer of sp^2 hybridized carbon atoms resulting in a hexagonal packed structure with two atoms per unit cell. Around each carbon atom, three strong σ bonds are established with the other three surrounding carbon atoms.[10]

The band structure of graphene consists of six Dirac cones in the hexagonal Brillouin zone.[11,12] The zero band gap of the graphene sheets renders the construction of graphene based field effect transistors very difficult. Therefore, several groups have proposed different methods to open a band gap in graphene.[13–25] Denis et al.[15] found that when graphene is doped with sulfur a band gap is opened depending on the sulfur concentration.[15] It is found that graphene is more accessible to doping

*Author to whom correspondence should be addressed.
Email: maalidph@yahoo.co.uk

and chemical modification at the same time is more susceptible to structural defects and impurities. Graphene is considered the most promising material for the adsorption of gases.[26–28] Recently a density functional theory (DFT) calculation was employed to investigate the use of transition metal doped carbon nanotubes for chemical gas sensing in pure and modified carbon structures.[29] Kozlov et al.[30] using DFT based Vienna *ab-inito* simulation package (VASP) calculation reported that by physisorbing molecules on graphene its electronic structure can be modified and band gaps can be induced. Moreover, the conditions for such band gap opening are well defined, and the size and character of the band gaps are tunable by varying the adsorbed molecule, its coverage, proximity to the graphene layer and by chemically changing the molecular electronic structure. Casolo et al.[31] have studied the effects substitutional defects such nitrogen and boron on the graphene electronic structure when they are periodically arranged to form some superlattices. Using group theoretical arguments and both tight binding (TB) and DFT calculations, they have shown that defects can either preserve the Dirac cones or open a band gap, depending on the superlattice symmetry (D6h and D3h, respectively). Specifically, honeycomb-shaped superlattices of boron or nitrogen atoms give rise to *p*- and *n*-doped graphene, respectively, preserving the Dirac cones. Janthon et al.[32] studied the accuracy of several DFT methods using van der Waals functional or dispersive forces corrections when describing the attachment of graphene on Ni(111). They found that the predictions made by different methodologies differ significantly and optB86b-vdW functional and Grimme dispersion correction seem to provide the best balanced description of stability of physisorption and chemisorption states. The attachment strength of the latter on Ni(111) surface, the graphene-Ni(111) separation, and the band structure of chemisorbed graphene was reported. Sharma and Verma[33] exploited the adsorption potential of pure and doped graphene for H_2S molecule using DFT modeling. Boron, aluminium and gallium atoms (group IIIB) are used as dopants. For each pure and doped graphene system optimum position of adsorbed H_2S molecule is determined and adsorption energies were calculated.

The electrons propagating through the graphene have a linear relation between energy and momentum and behave as massless Dirac fermions.[11, 34, 35] Thus it enables ultra wide-band tunability. Therefore, graphene shows very good optical transparency, and it can be optically visualized despite being only a single atom thick.[36] As a consequence of Pauli blocking, caused by the linear dispersion of the Dirac electrons in graphene, a broadband saturable absorption in graphene was observed. Thus graphene became suitable for applications in ultrafast mode locked lasers.[37–40] Mikhailov[41] reported that the massless energy spectrum of electrons and holes in graphene leads to the strongly nonlinear electromagnetic response of this system. Thus the author predicts that the graphene layer, irradiated by electromagnetic waves, emits radiation at higher frequency harmonics and can work as a frequency multiplier. The operating frequency of the graphene frequency multiplier can be in a broad range from microwaves to the infrared. Hong et al.[42] report strong third-harmonic generation in monolayer graphene grown by chemical vapor deposition (CVD) and transferred to an amorphous silica (glass) substrate. The photon energy is a three photon resonance with the exciton-shifted van Hove singularity at the M point of graphene. The polarization selection rules are derived and experimentally verified. Obraztsov et al.[43] reported that a strong and broadband light absorption in graphene allows one to achieve high carrier densities essential for observation of nonlinear optical (NLO) phenomena. They proposed and experimentally verified that a novel all-optical technique to induce the ultrafast photocurrents in unbiased graphene. The technique is solely based on photon-drag phenomena and provides full and non-contact control of the direction, amplitude as well as temporal profile of the photocurrent in graphene. This opens a very exciting opportunity to generate electromagnetic signals of prescribed waveform utilizing hot carrier dynamics and momentum relaxation in graphene. Wu et al.[44] propose a new scheme based on bilayer graphene (BLG) as a nonlinear optical material with an extremely large second order optical susceptibility $\chi^{(2)}_{ijk}(\omega) \sim 105$ pm/V. They found that this enhancement arises from two different types of quantum enhanced mechanisms, unique to the electronic structure of BLG. Their calculation shows an excellent electrical tunability of the optical nonlinearity in both intensity and wavelength compared to conventional nonlinear crystals. Recently some experiments[45–47] show that the nonlinear generation could be detected even through single layer graphene. Klekachev et al.[48] have performed an analysis of pristine graphene samples and compared the outcome with the response of CVD transferred graphene. In both type of samples, similar emission intensity is observed from single to bilayer/multilayers regions. They benchmark transferred CVD graphene towards exfoliated graphene by 2PF microscopy. On the other hand, for the second-harmonic signals, no effect is observed for CVD transferred graphene, while a different polarization pattern is observed for pristine samples. Gu et al.[49] perform first-principles calculations to study the high-order harmonic generation (HHG) induced in graphene nanostructures by the laser field. They presented a theoretical approach to investigate the HHG in the nano-graphene molecules. Bykov et al.[50] perform nonlinear optics (NLO) studies and NLO microscopy of multilayer graphene films deposited by CVD technique on glass and silicon substrates. Two characteristic spatial scales of several microns and hundreds of nanometers are observed, which are associated with flat graphene crystal domains and with the

cross section of the wrinkles that separate the domains. The second harmonic imaging microscopy (SHIM) show that the second-order nonlinear response originates primarily from the wrinkles and is probably due to local symmetry breaking associated with mechanical stress, charge, and thickness inhomogeneities. Dean and Driel[45] have measured the second-harmonic generation (SHG) from graphene and other graphitic films, from two layers to bulk graphite, at room temperature. Optical SHG of 800 nm, 150 fs fundamental pulses is observed from exfoliated graphene and multilayer graphitic films mounted on an oxidized silicon (001) substrate. The SHG anisotropy was observed as the sample rotated about the surface normal. For *p*-polarized fundamental and SHG light, the isotropic SHG from a graphene layer only slightly interferes with the fourfold symmetric response of the underlying substrate, while other samples show a threefold symmetry characteristic of significant SHG in the multilayer graphitic films. The dominance of the threefold anisotropy was maintained from bilayer graphene to bulk graphite.

It is worth exploring which atomic sites favor a good adsorption of H_2S on graphene sheet. Thus in this paper we study the adsorption of H_2S molecule on bilayer pristine graphene (BLPG), and the three possible adsorption sites of H_2S single molecule on single sheet of BLPG (top, bridge, and hollow) by using the density-functional theory (DFT) in an effort to calculate the different properties that might get changed after the adsorption. Also we investigate whether pristine graphene is a good adsorbent material for H_2S molecule or not, in order to use it as a novel generation of small gas molecules sensors. This motivated us to perform comprehensive calculation for the linear and nonlinear optical susceptibilities of BLPG, using the all electron full potential linearized augmented plane wave method. Although there exist many calculations of the electronic properties of graphene, there is dearth of the calculated optical properties of the BLPG. Since graphene is nearly transparent to visible light, it may possess interesting optical properties. Therefore we have addressed ourselves to calculate the linear and the nonlinear optical susceptibilities of BLPG.

2. STRUCTURAL PROPERTIES AND COMPUTATIONAL DETAILS

In order to investigate the linear and nonlinear optical susceptibilities of BLPG (Fig. 1(a)), and the resulting structure of adsorbed H_2S molecule onto a single sheet of BLPG at different sites (top, bridge, and hollow—Figs. 1(b)–(e)), the all-electron full potential linearized augmented plane wave (FP-LAPW) method was used to solve the Kohn Sham DFT equations within the framework of the WIEN2k code.[51] The exchange and correlation energy treated through a general gradient approximation by Perdew-Burke-Ernzerhof (GGA-PBE) approach.[52] It is well-known that the pristine graphene is centrosymmetric

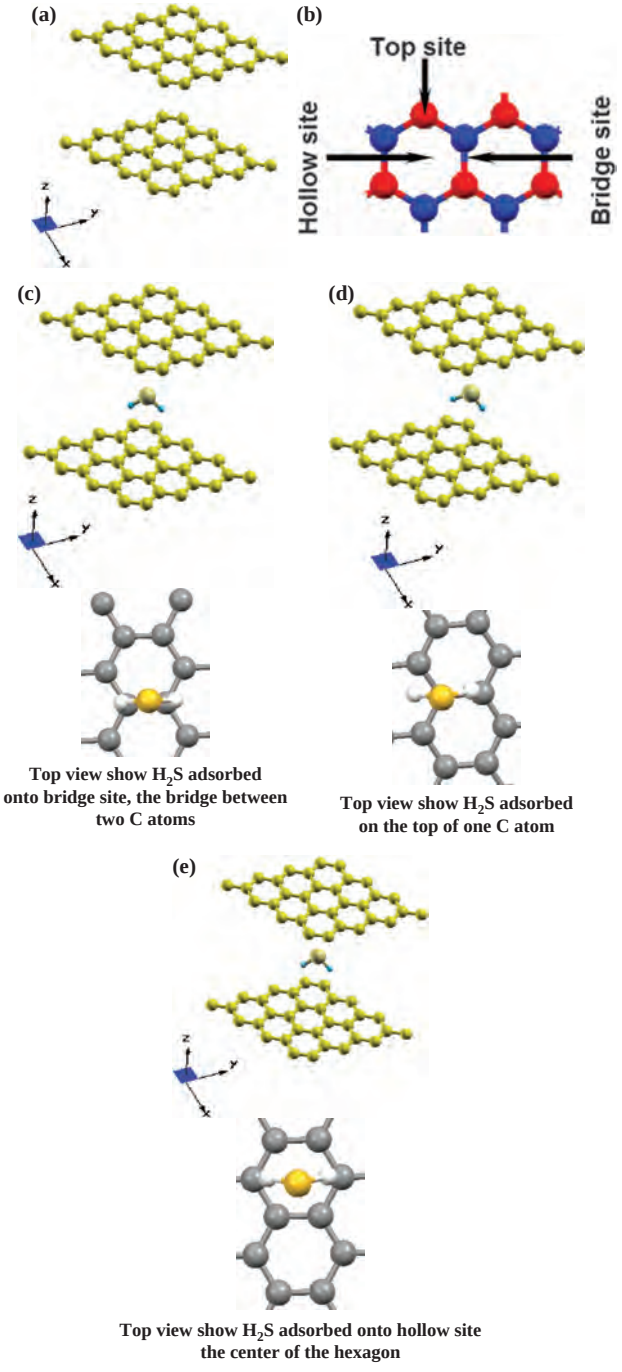

Fig. 1. Schematic view of; (a) BLPG; (b) Three different adsorption sites of H_2S on graphene; (c) H_2S adsorbed onto bridge site of single sheet of BLPG; (d) H_2S adsorbed onto top site of single sheet of BLPG; (e) H_2S adsorbed onto hollow site of single sheet of BLPG. The top view image shows the location of H_2S molecule with respect to the hexagon of the graphene sheet for the three different adsorption sites of H_2S on graphene sheet.

materials, has inversion symmetry and hence the second harmonic generation is symmetry-forbidden. We should emphasize that the inversion center in a crystalline structure is linked to parity as a conserved quantity.[53] Usually breaking of parity conservation in the atomic scale

structure can be achieved by external perturbations or by fabrication of specific structures at the atomic level.[54] Here we break the parity conservation in the atomic scale structure by fabrication of specific structures (adsorbing H_2S) at the atomic level (see Figs. 1(a)–(e)).

In order to achieve the self-consistency the muffin-tin radius (R_{MT}) was taken to be 1.33 a.u for C at pristine graphene (4×4) sheet, 1.27, 1.55, and 0.83 a.u for C, S and H atoms respectively for the top-, bridge-, and hollow-H_2S adsorbed on single sheet of BLPG. These values were chosen in such a way that the spheres did not overlap. In order to achieve sufficient energy convergence, the wave-functions in the interstitial regions were expanded in plane waves with a cutoff $K_{max} = 7.0/R_{MT}$, where R_{MT} denotes the smallest atomic sphere radius and K_{max} gives the magnitude of the largest K vector in the plane wave basis expansion. The maximum value of $\boldsymbol{l}$ was taken as $\boldsymbol{l}_{max} = 10$, while the charge density was Fourier expanded up to $G_{max} = 20$ (a.u)$^{-1}$. For calculating the linear and nonlinear optical susceptibilities a denser mesh of 800 **k**-points was used. The self-consistent calculations were considered to be converged when the total energy of the system is stable within 10^{-5} Ry. We should emphasize that the most stable adsorption configuration is the one with the lowest total energy and the highest adsorption energy among other adsorption sites.[55] Thus the top site (total energy $E_{TOT} = -3238.87878541$ Ryd) is the most stable configuration in comparison to hollow ($E_{TOT} = -3238.1058284$ Ryd) and bridge ($E_{TOT} = -3238.79501144$ Ryd).

Since the honeycomb two dimensional lattice of a monolayer carbon atoms has hexagonal symmetry, we need two dielectric tensor component to completely characterize the linear optical properties. These are $\varepsilon_2^{\perp}(\omega)$ and $\varepsilon_2^{\shortparallel}(\omega)$ the imaginary part of the frequency dependent complex dielectric functions, corresponding to electric vector $\vec{E}$ parallel or perpendicular to the **c** axis. We have performed calculations of the imaginary part of the inter-band frequency dependent dielectric function using the expressions[56]

$$\varepsilon_2^{\shortparallel}(\omega) = \frac{12}{m\omega^2}\int_{BZ}\sum_{nn'}\frac{|P^Z_{nn'}(k)|^2\, dS_k}{\nabla\omega_{nn'}(k)} \tag{1}$$

$$\varepsilon_2^{\perp}(\omega) = \frac{6}{m\omega^2}\int_{BZ}\sum_{nn'}\frac{[|P^X_{nn'}(k)|^2 + |P^Y_{nn'}(k)|^2]\, dS_k}{\nabla\omega_{nn'}(k)} \tag{2}$$

The above expressions are written in atomic units with $e^2 = 1/m = 2$ and $\hbar = 1$. Where $\hbar\omega$ is the photon energy. $P^X_{nn'}(k)$ and $P^Z_{nn'}(k)$ are the X and Z component of the dipolar matrix elements between initial $|nk\rangle$ and final $|n'k\rangle$ states with their eigenvalues $E_n(k)$ and $E_{n'}(k)$, respectively. $\omega_{nn'}(k)$ is the inter-band energy difference

$$\omega_{nn'}(k) = E_n(k) - E_{n'}(k) \tag{3}$$

and S_k is a constant energy surface.

$S_k = \{k; \omega_{nn'}(k) = \omega\}$. The integral is over the first Brillouin zone.

The real parts $\varepsilon_1(\omega)$ of the frequency dependent dielectric function can be derived from the imaginary part using the Kramers–Kronig relations.[57] The reflectivity $R(\omega)$, the absorption coefficient $I(\omega)$, refractive index $n(\omega)$, and extinction coefficient $k(\omega)$ are related to the reflectivity at normal incidence by[57]

$$R(\omega) = \frac{n + ik - 1}{n + ik + 1} \tag{4}$$

$$I(\omega) = \sqrt{2}\omega[\sqrt{\varepsilon_1(\omega)^2 + \varepsilon_2(\omega)^2} - \varepsilon_1(\omega)]^{1/2} \tag{5}$$

$$k(\omega) = I(\omega)/2\omega \tag{6}$$

$$n(\omega) = (1/\sqrt{2})[\sqrt{\varepsilon_1(\omega)^2 + \varepsilon_2(\omega)^2} + \varepsilon_1(\omega)]^{1/2} \tag{7}$$

The complex second-order nonlinear optical susceptibility tensor $\chi^{(2)}_{ijk}(-2\omega; \omega; \omega)$ can be generally written as:[58–61]

$$\chi^{ijk}_{\text{inter}}(-2\omega;\omega,\omega) = \frac{e^3}{\hbar^2}\sum_{nml}\int\frac{d\vec{k}}{4\pi^3}\frac{\vec{r}^i_{nm}\{\vec{r}^j_{ml}\vec{r}^k_{ln}\}}{(\omega_{ln}-\omega_{ml})}\left\{\frac{2f_{nm}}{(\omega_{mn}-2\omega)} + \frac{f_{ml}}{(\omega_{ml}-\omega)} + \frac{f_{ln}}{(\omega_{ln}-\omega)}\right\} \tag{8}$$

$$\chi^{ijk}_{\text{intra}}(-2\omega;\omega,\omega) = \frac{e^3}{\hbar^2}\int\frac{d\vec{k}}{4\pi^3}\left[\sum_{nml}\omega_{nm}\vec{r}^i_{nm}\{\vec{r}^j_{ml}\vec{r}^k_{ln}\} \times\left\{\frac{f_{nl}}{\omega^2_{ln}(\omega_{ln}-\omega)} - \frac{f_{lm}}{\omega^2_{ml}(\omega_{ml}-\omega)}\right\} - 8i\sum_{nm}\frac{f_{nm}\vec{r}^i_{nm}\{\Delta^j_{mn}\vec{r}^k_{nm}\}}{\omega^2_{mn}(\omega_{mn}-2\omega)} + 2\sum_{nml}\frac{f_{nm}\vec{r}^i_{nm}\{\vec{r}^j_{ml}\vec{r}^k_{ln}\}(\omega_{ml}-\omega_{ln})}{\omega^2_{mn}(\omega_{mn}-2\omega)}\right] \tag{9}$$

$$\chi^{ijk}_{\text{mod}}(-2\omega;\omega,\omega) = \frac{e^3}{2\hbar^2}\int\frac{d\vec{k}}{4\pi^3}\left[\sum_{nml}\frac{f_{nm}}{\omega^2_{mn}(\omega_{mn}-\omega)} \times\{\omega_{nl}\vec{r}^i_{lm}\{\vec{r}^j_{mn}\vec{r}^k_{nl}\} - \omega_{lm}\vec{r}^i_{nl}\{\vec{r}^j_{lm}\vec{r}^k_{mn}\}\} - i\sum_{nm}\frac{f_{nm}\vec{r}^i_{nm}\{\vec{r}^j_{mn}\Delta^k_{mn}\}}{\omega^2_{mn}(\omega_{mn}-\omega)}\right] \tag{10}$$

From these formulae we can notice that there are three major contributions to $\chi^{(2)}_{ijk}(-2\omega; \omega; \omega)$: the inter-band transitions $\chi^{ijk}_{\text{inter}}(-2\omega; \omega, \omega)$, the intra-band transitions $\chi^{ijk}_{\text{intra}}(-2\omega; \omega, \omega)$ and the modulation of inter-band terms by intra-band terms $\chi^{ijk}_{\text{mod}}(-2\omega; \omega, \omega)$, where $n \neq m \neq l$. Here n denotes the valence states, m the conduction states and l denotes all states ($l \neq m, n$). There are two kinds of transitions take place one of them vcc', involves one valence band (v) and two conduction bands (c and c'), and the second transition $vv'c$, involves two valence bands (v and v') and one conduction band (c). The symbols are defined as $\Delta^i_{nm}(\vec{k}) = \vartheta^i_{nn}(\vec{k}) - \vartheta^i_{mm}(\vec{k})$

Article

with $\vec{\vartheta}^{i}_{nm}$ being the i component of the electron velocity given as $\vartheta^{i}_{nm}(\vec{k}) = i\omega_{nm}(\vec{k})r^{i}_{nm}(\vec{k})$ and $\{r^{i}_{nm}(\vec{k})r^{j}_{ml}(\vec{k})\} = (1/2)(r^{i}_{nm}(\vec{k})r^{j}_{ml}(\vec{k}) + r^{j}_{nm}(\vec{k})r^{i}_{ml}(\vec{k}))$. The position matrix elements between band states n and m, $r^{i}_{nm}(\vec{k})$, are calculated from the momentum matrix element P^{i}_{nm} using the relation:[62] $r^{i}_{nm}(\vec{k}) = P^{i}_{nm}(\vec{k})/(im\omega_{nm}(\vec{k}))$, with the energy difference between the states n and m given by $\hbar\omega_{nm} = \hbar(\omega_n - \omega_m)$. $f_{nm} = f_n - f_m$ is the difference of the Fermi distribution functions. It has been demonstrated by Aspnes[63] that only the one-electron virtual transitions (transitions between one valence band state and two conduction band states) give a significant contribution to the second-order tensor. We ignore the virtual-hole contribution (transitions between two valence band states and one conduction band state) because it was found to be negative and more than an order of magnitude smaller than the virtual-electron contribution for this compound. For simplicity we denote $\chi^{(2)}_{ijk}(-2\omega;\omega;\omega)$ by $\chi^{(2)}_{ijk}(\omega)$. The subscripts i, j, and k are Cartesian indices.

3. RESULTS AND DISCUSSION

3.1. Electronic Band Structures

The electronic band structure's dispersion of BLPG and the three possible adsorption sites of H_2S single molecule on single sheet of BLPG (top, bridge, and hollow) in **k**-space along the high symmetry directions in the irreducible Brillouin zone (IBZ) are shown in Figure 2. In bridge site the H_2S single molecule is adsorbed in the middle of two carbon atoms, top site the H_2S adsorbed onto one C atom, while in the hollow site H_2S adsorbed at the center of a carbon hexagon (see Fig. 1(b)).

Following Figure 2, it is clear that the BLPG is zero gap semiconductor due to valence and conduction bands crossing at K point of BZ (Fig. 2(a)). However when we adsorb H_2S onto bridge site of single sheet of BPLG a dramatic changes occur in the dispersion of the electronic band structure resulting in opening a small direct energy gap of about 0.1 eV around Fermi energy (E_F) at M point of BZ (Fig. 2(b)). This is attributed to the fact that the adsortion of H_2S on bridge site causes strong hybridization between C-p and H-s, S-s/p states at the valence band maximum (VBM) and hence strong covalent bonds, while at the conduction band minimum (CBM) the hybridization is weaker and the bonds too. In adsorbed H_2S on the top site of single sheet of BPLG causes to push the conduction band minimum (CBM) further towards higher energies resulting in a bigger direct energy band gap of about 0.3 eV around K point of BZ (Fig. 2(c)). Adsorbing H_2S on top site causes very strong hybridization between C-p and H-s, S-s/p states at the VBM resulting in very strong covalent bonds, while at the CBM the hybridization is much weaker which leads to weak bonds. The upper valence band (Figs. 2(a)–(d)) shows a very flat k-dispersion. This reflects the low mobility of the holes. When H_2S is adsorbed on the hollow site of single sheet of BPLG we noticed that both of the CBM and VBM move towards each other and overlap around E_F.

3.2. Linear Optical Susceptibilities

The inter-band transitions of the dielectric function $\varepsilon(\omega)$ are usually presented as a superposition of direct and indirect transitions. We can neglect the indirect inter-band transitions formed by electron–phonon interactions that are expected to give a small contribution to $\varepsilon(\omega)$.[64] To calculate the direct inter-band contributions to the imaginary part of the dielectric function $\varepsilon_2(\omega)$, it is necessary to perform summation over all possible transitions from occupied to unoccupied band states taking the appropriate inter-band transition matrix elements into account.

Figures 3(a)–(d), display the variation of the imaginary (responsible for absorption) part of the electronic dielectric function, $\varepsilon_2^{\parallel}(\omega)$ and $\varepsilon_2^{\perp}(\omega)$ for BLPG, bridge, top and hollow sites configurations of BLPG, respectively. For the calculation of the linear optical susceptibilities the half-width broadening (due to electron–phonon interactions) is taken to be 0.1 eV which is typical of the experimental accuracy.[65] To the best of our knowledge, there is a dearth experimental data and theoretical calculations for the optical properties of the BLPG, bridge, top and hollow sites configurations of BLPG to compare with our results. But we can refer to our previous work[61,66–70] in which we compared our calculated optical properties with the measured one to justify the reliability of the DFT methodology for the calculation of dielectric functions. Following Figures 3(a)–(d), one can notice that the $\varepsilon_2^{\perp}(\omega)$ component of BLPG, bridge, top and hollow sites configurations of BLPG show three major structures. For simplicity we call them as A, B, and C. The component $\varepsilon_2^{\parallel}(\omega)$ shows only one structure which we call it as D. Figure 3(a) illustrates the huge anisotropy between $\varepsilon_2^{\perp}(\omega)$ and $\varepsilon_2^{\parallel}(\omega)$ confirming that BLPG possessing an interesting optical properties.

Figure 3(b) shows the influence of adsorbing H_2S onto a single sheet of BPLG at bridge site which leads to a change in the optical properties due to the changes in the band structure and dipole matrix elements. As a results one can see that;

(i) All the structures are shifted towards higher energies by around 0.1 eV ($\sim E_g$) with respect to Figure 3(a).
(ii) Doubling of the amplitude of the structure A.
(iii) Reduction of the amplitude of the B structure and becoming wide with more peaks.
(iv) Reduction in the amplitude of D structure to overlap with C structure showing isotropic behavior.

When we adsorbed H_2S on top site of single sheet of BPLG (Fig. 3(c)) we notice that:

(i) All the structures are shifted towards higher energies by around 0.3 eV ($\sim E_g$) with respect to Figure 3(a).
(ii) The A structure becomes sharp with amplitude three times higher than that in Figure 3(a).

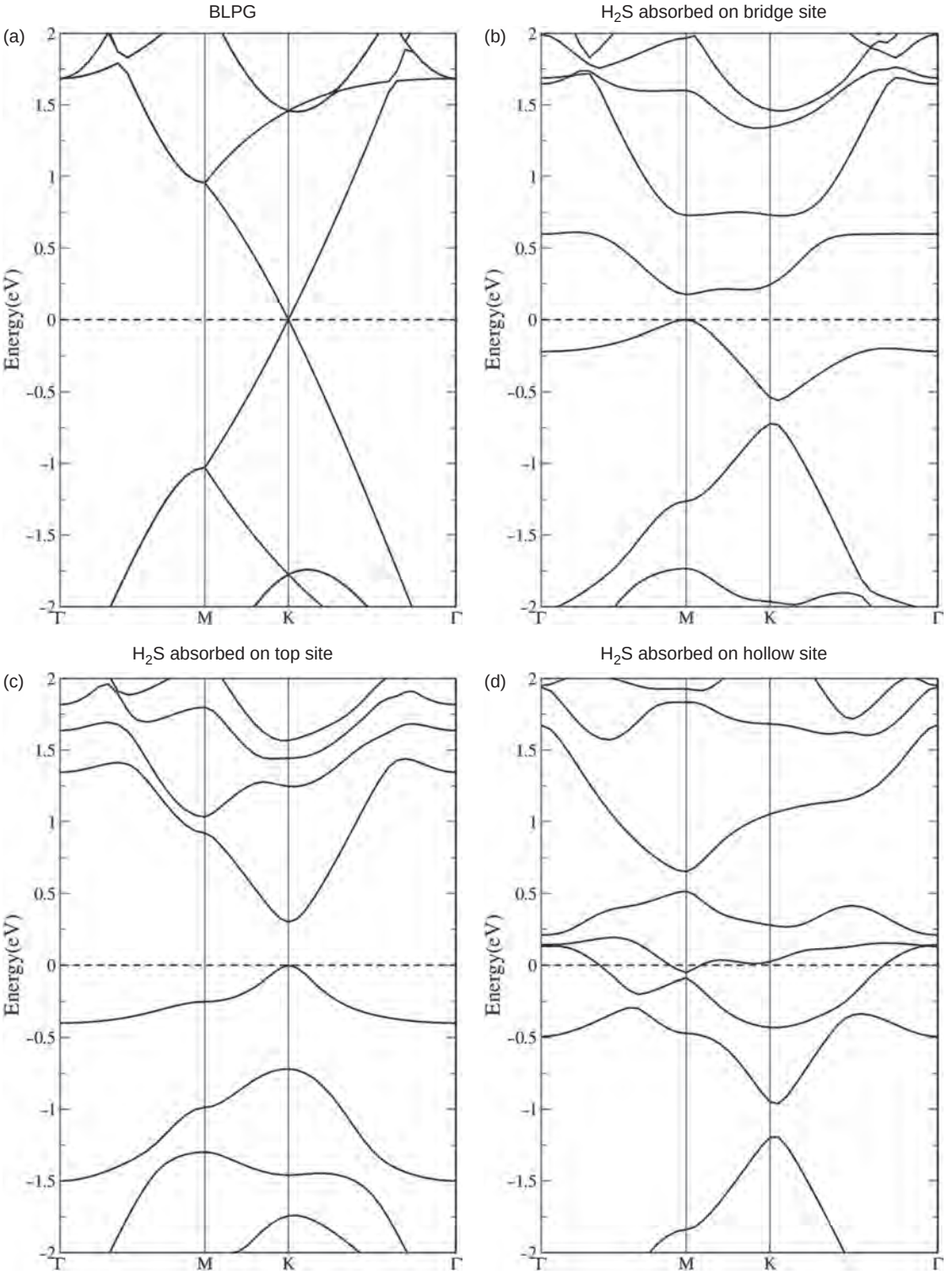

Fig. 2. Calculated electronic band structure; (a) BLPG; (b) H_2S adsorbed onto bridge site of single sheet of BLPG; (c) H_2S adsorbed onto top site of single sheet of BLPG; (d) H_2S adsorbed onto hollow site of single sheet of BLPG.

(iii) The B structure merges with the valley between structure A and B to show continuous wide structure.
(iv) The D structure shifts towards lower energies, two insignificant humps are observed at low energies.

Finally when H_2S adsorbed on hollow site of single sheet of BPLG (Fig. 3(d));
(i) A sharp rise appear below 1.0 eV due to intra band transitions.

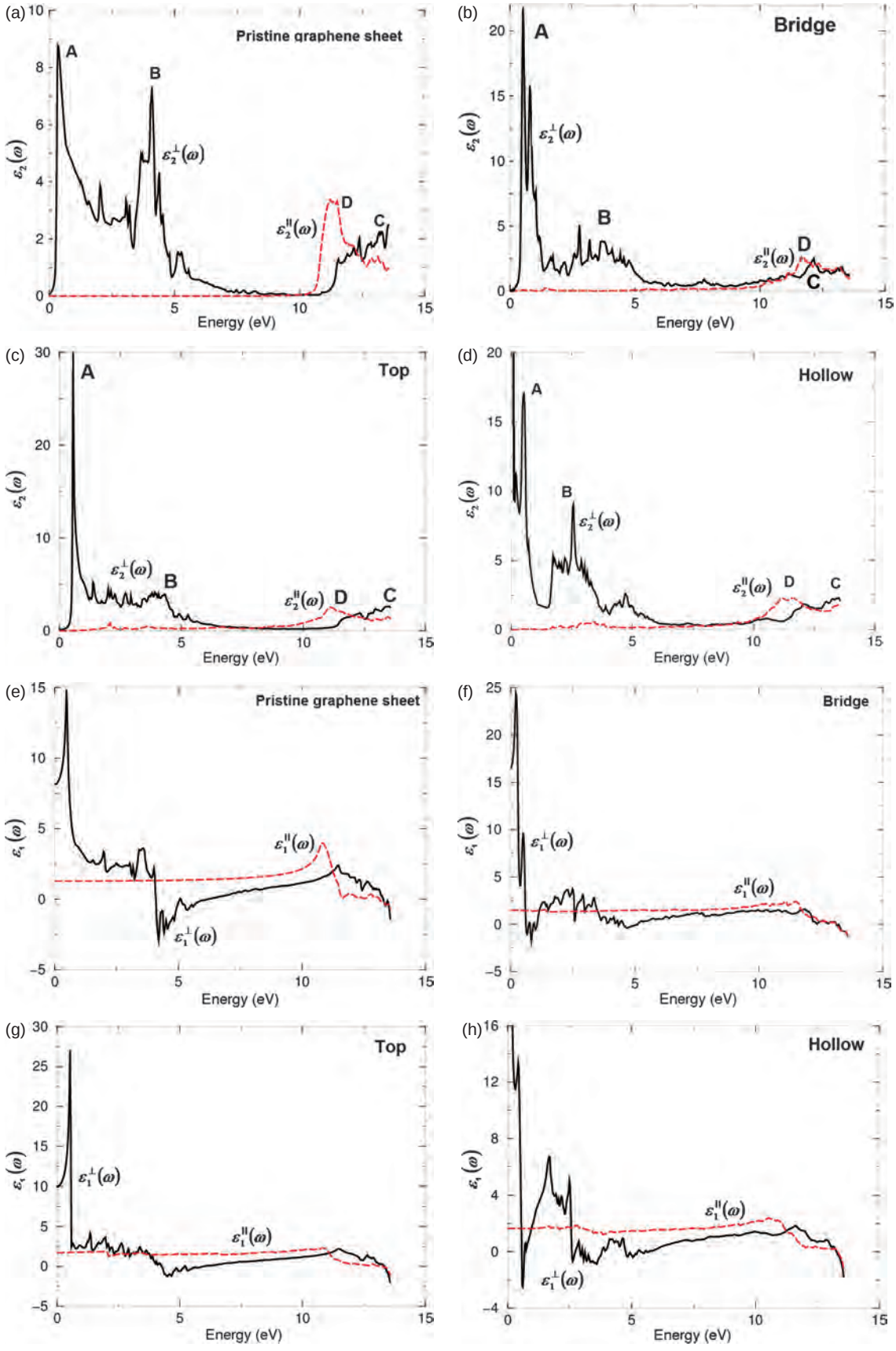

Fig. 3. Continued.

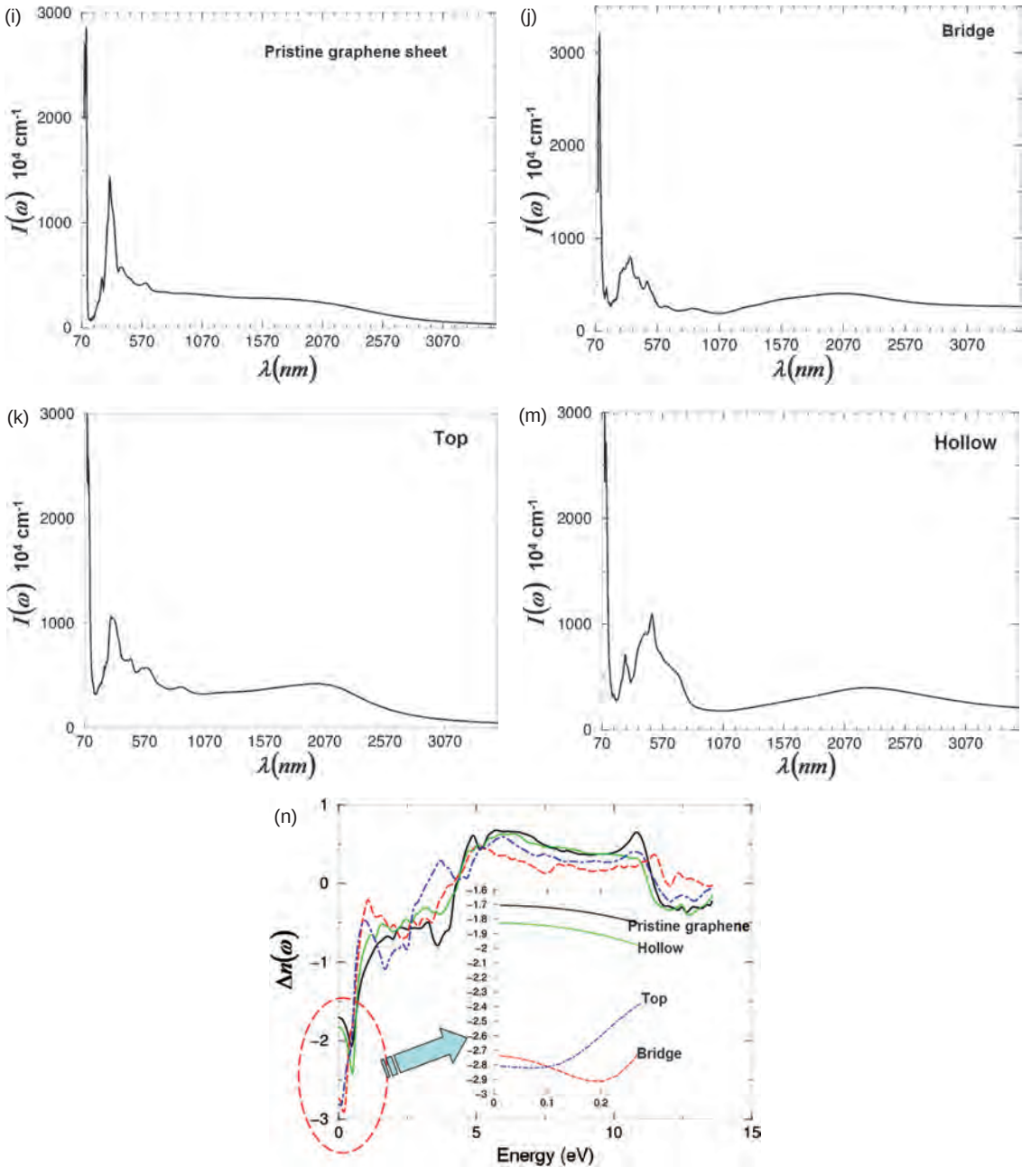

Fig. 3. Calculated $\varepsilon_2^{||}(\omega)$ and $\varepsilon_2^{\perp}(\omega)$ (a) BLPG; (b) H_2S adsorbed onto bridge site of single sheet of BLPG; (c) H_2S adsorbed onto top site of single sheet of BLPG; (d) H_2S adsorbed onto hollow site of single sheet of BLPG; Calculated $\varepsilon_1^{||}(\omega)$ and $\varepsilon_1^{\perp}(\omega)$ (e) BLPG; (f) H_2S adsorbed onto bridge site of single sheet of BLPG; (g) H_2S adsorbed onto top site of single sheet of BLPG; (h) H_2S adsorbed onto hollow site of single sheet of BLPG; Calculated $I(\omega) \times 10^4$ cm^{-1} as a function of the wavelengths for; (i) BLPG; (j) H_2S adsorbed onto bridge site of single sheet of BLPG; (k) H_2S adsorbed onto top site of single sheet of BLPG; (m) H_2S adsorbed onto hollow site of single sheet of BLPG; (n) Calculated $\Delta n(\omega)$ for pristine graphene, H_2S adsorbed onto bridge site of single sheet of BLPG, H_2S adsorbed onto top site of single sheet of BLPG, H_2S adsorbed onto hollow site of single sheet of BLPG.

(ii) Doubling of the amplitude of structure A with respect to Figure 3(a).
(iii) The amplitude of B structure is increased and a small hump appears on the right hand side of structure B.
(iv) The two small humps of $\varepsilon_2^{||}(\omega)$ which appears in Figure 3(c) are merged and the D structure shifted towards lower energies by around 0.5 eV.

In general the changes in the optical properties when one moves from BPLG to bridge, top and hollow sites of adsorbing H_2S onto single sheet of BPLG, is attributed to the fact that adsorbed H_2S on different sites onto single sheet of BPLG causes changes in the electronic structure (see Figs. 2(a)–(d)). The significant effect on the magnitude, peaks positions and the spectral structure of the

optical properties is according to the dipolar selection rule which allows only transitions corresponding to a change in the angular momentum quantum number l by unity.

Figures 3(e)–(h) illustrate the real parts $\varepsilon_1^{\parallel}(\omega)$ and $\varepsilon_1^{\perp}(\omega)$ of the frequency dependent dielectric functions. Again it shows huge anisotropy between the two polarizations confirming that BLPG is possesses interesting optical properties. The values of $\varepsilon_1^{\parallel}(0)$ and $\varepsilon_1^{\perp}(0)$ are listed in Table I.

It was observed experimentally that the optical absorption of graphene sheets to be proportional to the number of sheets, each absorbing can be expressed by $A \approx 1 - T \approx \pi\alpha \approx 2.3\%$ over the visible spectrum.[71–74] The absorption spectrum of graphene sheet is quite flat extended from 300 nm to 2500 nm with absorption peak in the UV region ($\sim$270 nm), which is due to exciton-shifted van Hove singularity in the graphene density of states.[71–74] Theoretically by using the FPLAPW method we have obtained the same observation as illustrated in Figures 3(i)–(m). For BLPG strong saturable absorption have been found because of large absorption and Pauli blocking.[38, 41]

Graphene exhibits a variety of transport phenomena that are characteristic of 2D Dirac fermions, such as a minimum conductivity of $\sim 4e^2/h$ even when the carrier concentration tends to zero,[34] and Shubnikov-de Haas oscillations with a π phase shift due to Berry's phase.[34]

In additional we have calculated the refractive index dispersions $n(\omega)$. The calculated values of $n^{\parallel}(0)$ and $n^{\perp}(0)$ are listed at Table I. The refractive indices show a considerable anisotropy which is important for second harmonic generation (SHG) and optical parametric oscillation (OPO) as it is defined by the phase-matching condition. The birefringence can be calculated from the linear response functions from which the anisotropy of the index of refraction is determined. The birefringence is the difference between the extraordinary and ordinary refraction indices, $\Delta n(\omega) = n_e(\omega) - n_o(\omega)$, where $n_o(\omega)$ is the index of refraction for an electric field oriented along the **c**-axis and $n_e(\omega)$ is the index of refraction for an electric field perpendicular to the **c**-axis. Figure 3(n) shows the birefringence $\Delta n(\omega)$ dispersion for pristine graphene, bridge, top and hollow respectively. It is clear that the birefringence is important only in the non-absorbing spectral range, which is below the energy gap. We find that BLPG, bridge, top and hollow possesses negative birefringence at the static limit, these values are listed in Table I.

Table I. Calculated $\varepsilon_1^{\parallel}(0)$, $\varepsilon_1^{\perp}(0)$, $n^{\parallel}(0)$, $n^{\perp}(0)$, $\Delta n(0)$, $R^{\parallel}(0)$, and $R^{\perp}(0)$.

Component	Pristine	Bridge	Top	Hollow
$\varepsilon_1^{\parallel}(0)$	1.50	2.0	1.9	–
$\varepsilon_1^{\perp}(0)$	6.10	16.65	10.0	–
$n^{\parallel}(0)$	1.19	1.21	1.31	1.30
$n^{\perp}(0)$	2.85	3.95	3.15	4.10
$\Delta n(0)$	−1.69	−2.74	−2.81	−1.83
$R^{\parallel}(0)$	0.01	0.01	0.02	0.02
$R^{\perp}(0)$	0.23	0.36	0.27	0.37

3.3. Nonlinear Optical Susceptibilities

The tensor $\chi_{ijk}^{(2)}$ describes the second-order nonlinear optical effect. This is a third rank tensor, in the electric dipole approximation; contain nonvanishing elements only for noncentrosymmetric crystalline structure. The third order nonlinear optical effects are described by the tensors $\chi_{ijkl}^{(3)}$ and γ_{ijkl} and no symmetry requirements are imposed on these effects to occur.[75] The BLPG, and H_2S adsorbed at bridge, top and hollow sites of the single sheet of BLPG processes several nonzero component. Thus we will concentrate only on the major components namely; 111, 121, 122, 211 for BLPG, and 131, 311, and 333 for bridge, top and hollow sites, (1, 2, and 3 refer to the x, y and z axes, respectively).[76] We should emphasize that 121 is the dominant component for BLPG, 311 for both of bridge and hollow sites and 131 for top site. These components show the highest value of $|\chi_{ijk}^{(2)}(\omega)|$ at both of static limit and at $\lambda = 1064$ nm among the others as illustrated in Figures 4(a)–(d) and listed in Table II. The calculated $|\chi_{ijk}^{(2)}(0)|$ and $|\chi_{ijk}^{(2)}(\omega)|$ at $\lambda = 1064$ nm for BLPG, and H_2S adsorbed onto bridge, top and hollow sites of the BLPG are evaluated and listed in Table II. The static values of the second order susceptibility tensor are very important and can be used to estimate the relative SHG efficiency.

To the best of our knowledge there is no experimental data for NLO susceptibilities of BLPG and H_2S single molecule adsorbed at three different sites onto a single graphene sheet of BPLG to compare with our theoretical results. We would like to mention here that in our previous works[60, 67, 68, 70, 77–79] we have calculated the linear and nonlinear optical susceptibilities using FPLAPW method of several systems whose linear and nonlinear optical susceptibilities are known experimentally. In these previous calculations we found very good agreement with the experimental data. Thus, we believe that our calculations reported in this paper would produce very accurate and reliable results.

From the calculated $\chi_{ijk}^{(2)}(\omega)$ dispersion we have obtained the microscopic first hyperpolarizability, β_{ijk}, the vector components along the dipole moment direction. The microscopic first hyperpolarizability terms cumulatively yields a bulk observable second order susceptibility term, $\chi_{ijk}^{(2)}(\omega)$, which in turn is responsible for the high SHG response.[60, 67, 68, 70, 76–80] For the dominant component $|\chi_{ijk}^{(2)}(\omega)|$ we have calculated β_{ijk} at the static limit and at$\lambda = 1064$ nm, using the expression give in Ref. [76].

$$\beta_{ijk} = \frac{\chi_{ijk}^{(2)}}{Nf^3} \tag{11}$$

where (N) is the number of molecules/cm^3 which about (0.125×10^{23}) and (f) is the local field factor, the value

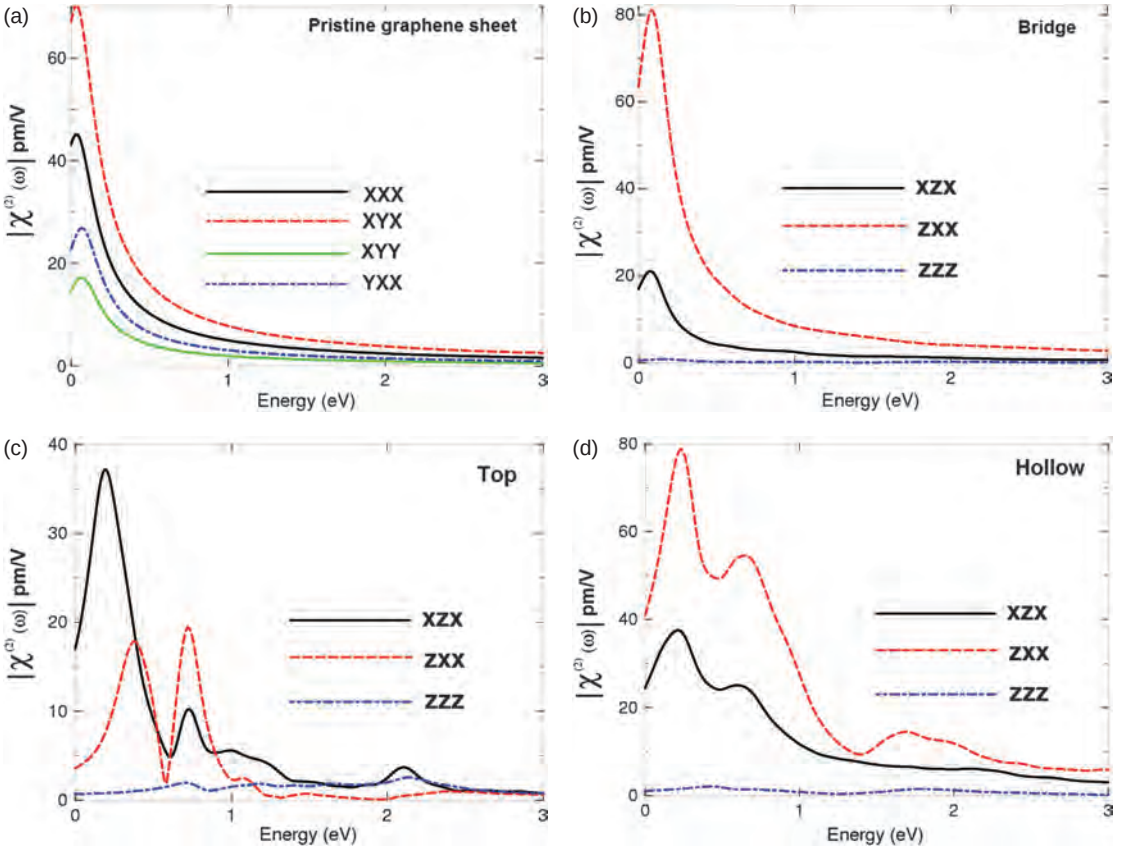

Fig. 4. Calculated $|\chi^{(2)}_{ijk}(\omega)|$; (a) BLPG; (b) H_2S adsorbed onto bridge site of single sheet of BLPG; (c) H_2S adsorbed onto top site of single sheet of BLPG; (d) H_2S adsorbed onto hollow site of single sheet of BLPG.

of (f) is 1.3, and $\chi^{(2)}_{ijk}$ is the value of the SHG (67.0×10^{-7} esu) at the static limit. Using this information we can estimate the value of first hyperpolarizability tensor β_{ijk}. Following Eq. (12), the value of β_{121} for BLPG is listed in Table II. Unfortunately we do not aware the values of the density for H_2S adsorbed onto bridge, top and hollow sites of graphene sheet of BLPG, in order to calculate the hyperpolarizability tensor β_{ijk}.

Table II. Calculated $|\chi^{(2)}_{ijk}(\omega)|$ in (pm/V) for BLPG, H_2S adsorbed onto bridge, top and hollow site of single sheet of BLPG along with the calculated values of first hyperpolarizability, β_{121} in (esu) for pristine graphene. The bold numbers are the values of the dominate components.

Component	Pristine	Bridge	Top	Hollow
$\lvert\chi^{(2)}_{111}(\omega)\rvert$	43.0	0.0	0.0	0.0
$\lvert\chi^{(2)}_{121}(\omega)\rvert$	**67.0**	0.0	0.0	0.0
$\lvert\chi^{(2)}_{122}(\omega)\rvert$	15.0	0.0	0.0	0.0
$\lvert\chi^{(2)}_{211}(\omega)\rvert$	23.0	0.0	0.0	0.0
$\lvert\chi^{(2)}_{131}(\omega)\rvert$	0.0	**17.5**	**17.6**	25.0
$\lvert\chi^{(2)}_{311}(\omega)\rvert$	0.0	3.5	3.6	**41.9**
$\lvert\chi^{(2)}_{333}(\omega)\rvert$	0.0	0.6	0.7	0.8
β_{ijk}	β_{121} 243.24×10^{-30}	β_{131}	β_{131}	β_{311}

4. CONCLUSION

DFT calculations based on all-electron full potential linearized augmented plane wave method are used to investigate the linear and nonlinear optical properties of BLPG and H_2S adsorbed at three different sites onto single sheet of BLPG are calculated. The calculation show that adsorbed H_2S onto single graphene sheet of BLPG cause significant changes in the electronic structures and hence significant changes in the linear and nonlinear optical susceptibilities. The calculated linear optical properties show a huge anisotropy confirming that the BLPG possess unusual and interesting optical properties. We should emphasize that the anisotropy in the linear optical susceptibilities favors an enhanced phase matching conditions necessary for observation of the second harmonic generation and optical parametric oscillation. We find that the absorption spectrum of graphene sheet is quite flat extended from 300–2.500 nm with absorption peak in the UV region (~270 nm), which is in excellent agreement with the experimental data. The pristine graphene possesses a strong saturable absorption because of large absorption and Pauli blocking. We have calculated the nonlinear optical susceptibilities of BLPG and the three configurations and found that they possess a huge second harmonic generation. Also we have obtained the

microscopic hyperpolarizability, β_{ijk}, for BLPG. We would like to mention here that in our previous works we have calculated the linear and nonlinear optical susceptibilities using FPLAPW method on several systems whose linear and nonlinear optical susceptibilities are known experimentally. In those previous calculations we found very good agreement with the experimental data. Thus, we believe that our calculations reported in this paper would produce very accurate and reliable results.

Acknowledgments: The result was developed within the CENTEM project, reg. no. CZ.1.05/2.1.00/03.0088, co-funded by the ERDF as part of the Ministry of Education, Youth and Sports OP RDI program. Computational resources were provided by MetaCentrum (LM2010005) and CERIT-SC (CZ.1.05/3.2.00/08.0144) infrastructures. Sushil Auluck thanks Council of Scientific and Industrial Research (CSIR)—National Physical Laboratory for financial support.

References and Notes

1. C. Gomez-Navarro, M. Burghard, and K. Kern; Elastic properties of chemically derived single graphene sheets; *Nano Lett.* 8, 2045 (**2008**).
2. Y.-H. Lin, K. A. Jenkins, A. Valdes-Garcia, J. P. Small, D. B. Farmer, and P. Avouris; Operation of graphene transistors at gigahertz frequencies; *Nano Lett.* 9, 422 (**2009**).
3. C. L. Kane and E. J. Mele; Quantum spin hall effect in graphene; *Phys. Rev. Lett.* 95, 226801 (**2005**).
4. A. Ferre-Vilaplana; Numerical treatment discussion and *ab initio* computational reinvestigation of physisorption of molecular hydrogen on graphene; *J. Chem. Phys.* 122, 104709 (**2005**).
5. I. Zanella, S. B. Fagan, R. Mota, and A. Fazzio; Electronic and magnetic properties of Ti and Fe on graphene; *J. Phys. Chem. C* 112, 9163 (**2008**).
6. Z. Liu, J. T. Robinson, X. Sun, and H. Dai; PEGylated nanographene oxide for delivery of water insoluble cancer drugs; *J. Am. Chem. Soc.* 130, 10876 (**2008**).
7. A. de Leon and A. F. Jalbout; A 'Scorpion' like SWNT/carbon sheet molecular trap; *Chem. Phys. Lett.* 457, 179 (**2008**).
8. K. Nakada, M. Fujita, G. Dresselhaus, and M. S. Dresselhaus; Edge state in graphene ribbons: Nanometer size effect and edge shape dependence; *Phys. Rev. B: Condens. Mater. Phys.* 54, 17954 (**1996**).
9. S. Okada; Energetics of nanoscale graphene ribbons: Edge geometries and electronic structures; *Phys. Rev. B: Condens. Mater. Phys.* 77, 041408 (**2008**).
10. R. Lv and M. Terrones; Towards new graphene materials: Doped graphene sheets and nanoribbons; *Mater. Lett.* 78, 209 (**2012**).
11. P. R. Wallace; The band theory of graphite; *Phys. Rev.* 71, 622 (**1974**).
12. G. W. Semenoff; Condensed-matter simulation of a three-dimensional anomaly; *Phys. Rev. Lett.* 53, 2449 (**1984**).
13. R. M. Ribeiro, N. M. R. Peres, J. Coutinho, and P. R. Briddon; Inducing energy gaps in monolayer and bilayer graphene: Local density approximation calculations; *Phys. Rev. B: Condens. Mater. Phys.* 78, 075442 (**2008**).
14. E. Bekyarova, M. E. Itkis, P. Ramesh, C. Berger, M. Sprinkle, W. A. De Heer, and R. C. Haddon; Chemical modification of epitaxial graphene: Spontaneous grafting of aryl groups; *J. Am. Chem. Soc.* 131, 1336 (**2009**).
15. P. A. Denis, R. Faccio, and A. W. Mombru; Is it possible to dope single-walled carbon nanotubes and graphene with sulfur?; *Chem. Phys. Chem.* 10, 715 (**2009**).
16. D. C. Elias, R. R. Nair, T. M. G. Mohiuddin, S. V. Morozov, P. Blake, M. P. Halshall, A. C. Ferrari, D. W. Boukhvalov, M. I. Katsnelson, A. K. Geim, and K. S. Novoselov; Fine structure constant defines visual transparency of graphene; *Science* 323, 610 (**2009**).
17. J. O. Sofo, A. S. Chaudhari, and G. D. Barber; Graphane: A two-dimensional hydrocarbon; *Phys. Rev. B* 75, 153401 (**2007**).
18. S. Casolo, O. L. Lovnik, R. Martinazzo, and G. F. Tantardini; Understanding adsorption of hydrogen atoms on graphene; *J. Chem. Phys.* 130, 054704 (**2009**).
19. D. W. Boukhvalov, M. I. Katsnelson, and A. I. Lichtenstein; Hydrogen on graphene: Electronic structure, total energy, structural distortions and magnetism from first-principles calculations; *Phys. Rev. B: Condens. Mater. Phys.* 77, 035427 (**2008**).
20. X. Sha and B. Jackson; First-principles study of the structural and energetic properties of H atoms on a graphite (0 0 0 1) surface; *Surf. Sci.* 496, 318 (**2002**).
21. L. Hornekaer, E. Rauls, W. Xu, Z. Sljivancanin, R. Otero, I. Steensgaard, E. Laegsgaard, B. Hammer, and F. Besenbacher; Metastable structures and recombination pathways for atomic hydrogen on the graphite (0001) surface; *Phys. Rev. Lett.* 96, 156104 (**2006**).
22. Y. Ferro, F. Marinelli, and A. Allouche; Density functional theory investigation of the diffusion and recombination of H on a graphite surface; *Chem. Phys. Lett.* 368, 609 (**2003**).
23. T. Roman, W. A. Dino, H. Nakanishi, H. Kasai, T. Sugimoto, and K. Tange; Hydrogen pairing on graphene; *Carbon* 45, 218 (**2007**).
24. L. Chen, A. C. Copper, C. P. Pez, and H. Cheng; Mechanistic study on hydrogen spillover onto graphitic carbon materials; *J. Phys. Chem. C* 111, 18995 (**2007**).
25. P. O. Lehtinen, A. S. Foster, Y. Ma, A. V. Krasheninnikov, and R. M. Nieminen; Irradiation-induced magnetism in graphite: A density functional study; *Phys. Rev. Lett.* 93, 187202 (**2004**).
26. M. Suzuki; Activated carbonfiber: Fundamentals and applications; *Carbon* 32, 577 (**1994**).
27. J. Zhao, A. Buldum, J. Han, and J. P. Lu; Gas molecule adsorption in carbon nanotubes and nanotube bundles; *Nanotechnology* 13, 195 (**2002**).
28. P. Bondavalli, P. Legagneux, and D. Pribat; Carbon nanotubes based transistors as gas sensors: State of the art and critical review; *Sens. Actuators B* 140, 304 (**2009**).
29. J. M. Garcia-Lastra, D. J. Mowbray, K. S. Thygesen, A. Rubio, and K. W. Jacobsen; Modeling nanoscale gas sensors under realistic conditions: Computational screening of metal-doped carbon nanotubes; *Phys. Rev. B: Condens. Mater. Phys.* 81, 245429 (**2010**).
30. S. M. Kozlov, F. Viñes, and A. Görling; Bandgap engineering of graphene by physisorbed adsorbates; *Adv. Mater.* 23, 2638 (**2011**).
31. S. Casolo, R. Martinazzo, and G. F. Tantardini; Band engineering in graphene with superlattices of substitutional defects; *J. Phys. Chem. C* 115, 3250 (**2011**).
32. P. Janthon, F. Viñes, S. M. Kozlov, J. Limtrakul, and F. Illas; Theoretical assessment of graphene-metal contacts; *J. Chem. Phys.* 138, 244701 (**2013**).
33. S. Sharma and A. S.Verma; A theoretical study of H_2S adsorption on graphene doped with B, Al and Ga; *Physica B* 427, 12 (**2013**).
34. A. K. Geim and K. S. Novoselov; The rise of graphene; *Nature Mater.* 6, 183 (**2007**).
35. J. C. Charlier, P. C. Eklund, J. Zhu, and A. C. Ferrari; Electron and phonon properties of graphene: Their relationship with carbon nanotubes; *Top. Appl. Phys.* 111, 673 (**2008**).

36. P. Blake, E. W. Hill, A. H. C. Neto, K. S. Novoselov, D. Jiang, R. Yang, T. J. Booth, and A. K. Geim; Making graphene visible; *Appl. Phys Lett* 91, 063124 **(2007)**.
37. Z. Sun, T. Hasan, F. Torrisi, D. Popa, G. Privitera, F. Wang, F. Bonaccorso, D. M. Basko, and A. C. Ferrari; Graphene mode-locked ultrafast laser; *ACS Nano* 4, 803 **(2010)**.
38. Q. Bao, H. Zhang, Y. Wang, Z. Ni, Y. Yan, Z. X. Shen, K. P. Loh, and D. Y. Tang; Atomic-layer graphene as a saturable absorber for ultrafast pulsed lasers; *Adv. Funct. Mater.* 19, 3077 **(2009)**.
39. Q. Bao, H. Zhang, J.-X. Yang, S. Wang, D. Y. Tang, Rajan Jose, Seeram Ramakrishna, C. T. Lim, and K. P. Loh; Graphene-polymer nanofiber membrane for ultrafast photonics; *Adv. Funct. Mater.* 20, 782 **(2010)**.
40. H. Zhang, D. Tang, R. J. Knize, L. Zhao, Q. Bao, and K. P. Loh; Graphene mode locked, wavelength-tunable, dissipative soliton fiber laser; *Appl. Phys. Lett.* 96, 111112 **(2010)**.
41. S. A. Mikhailov; Non-linear electromagnetic response of graphene; *Europhys. Lett.* 79, 27002 **(2007)**.
42. S.-Y. Hong, J. I. Dadap, N. Petrone, P.-C. Yeh, J. Hone, and R. M. Osgood, Jr.; Optical third-harmonic generation in graphene; *Phys. Rev. X* 3, 021014 **(2013)**.
43. P. A. Obraztsov, T. Kaplas, S. V. Garnov, M. Kuwata-Gonokami, A. N. Obraztsov, and Y. P. Svirko; All-optical control of ultrafast photocurrents in unbiased graphene; *Scientific Reports* 4, 4007 **(2014)**.
44. S. Wu, L. Mao, A. M. Jones, W. Yao, C. Zhang, and X. Xu; Quantum-enhanced tunable second-order optical nonlinearity in bilayer graphene; *Nano Lett.* 12, 2032 **(2012)**.
45. J. J. Dean and H. M. van Driel; Graphene and few-layer graphite probed by second-harmonic generation: Theory and experiment; *Phys. Rev. B: Condens. Mater. Phys.* 82, 125411 **(2010)**.
46. J. J. Dean and H. M. van Driel; Second harmonic generation from graphene and graphitic films; *Appl. Phys. Lett.* 95, 261910 **(2009)**.
47. E. Hendry, P. J. Hale, J. Moger, and A. K. Savchenko, and S. A. Mikhailov; Coherent nonlinear optical response of graphene; *Phys. Rev. Lett.* 105, 097401 **(2010)**.
48. A. V. Klekachev, I. Asselberghs, C. Huyghebaert, M. Vanbel, M. A. Van der Veen, A. L. Stesmans, M. M. Heyns, S. De Gendt, and T. Verbiest; Optical processes in organic materials and nanostructures, *Proceedings of the SPIE* **(2012)**, Vol. 8474, p. 8, article id. 847405.
49. M. Gu, G. Zhang, and X. Wu; Laser induced multiphoton effects in nano-graphene molecules; *Appl. Sci.* 3, 278 **(2013)**.
50. A. Y. Bykov, P. S. Rusakov, E. D. Obraztsova, and T. V. Murzina; Probing structural inhomogeneity of graphene layers via nonlinear optical scattering; *Opt. Lett.* 38, 4589 **(2013)**.
51. P. Blaha, K. Schwarz, G. K. H . Madsen, D. Kvasnicka, and J. Luitz, WIEN2K, "An augmented plane wave + local orbitals program for calculating crystal properties," Karlheinz Schwarz, Techn. Universitat, Wien, Austria **(2001)**, ISBN 3-9501031-1-2.
52. J. P. Perdew, S. Burke, and M. Ernzerhof; Generalized gradient approximation made simple; *Phys. Rev. Lett.* 77, 3865 **(1996)**.
53. R. P. Feynman, R. B. Leighton, and M. Sands; The Feynman Lectures on Physics, Addison-Wesley Publishing Company, Massachusetts **(1963)**, Vol. 3.
54. J. Yan, T. Villarson, E. A. Henriksen, P. Kim, and A. Pinczuk; Optical phonon mixing in bilayer graphene with a broken inversion symmetry; *Phys. Rev. B: Condens. Mater. Phys.* 80, 241417 **(2009)**.
55. M. Zhou, Y.-H. Lu, Y.-Q. Cai, C. Zhang, and Y.-P. Feng; Adsorption of gas molecules on transition metal embedded graphene: A search for high-performance graphene-based catalysts and gas sensors; *Nanotechnology* 22, 385502 **(2011)**.
56. S. Hufner, R. Claessen, F. Reinert, Th. Straub, V. N. Strocov, and P. Steiner; Photoemission spectroscopy in metals: Band structure-Fermi surface-spectral function; *J. Electron Spectra. Relat. Phenom.* 100, 191 **(1999)**.
57. F. Wooten, Optical Properties of Solids, Academic press, New York and London **(1972)**.
58. S. Sharma, J. K. Dewhurst, and C. Ambrosch-Draxl; Linear and second-order optical response of III–V monolayer superlattices; *Phys. Rev. B: Condens. Mater. Phys.* 67, 165332 **(2003)**.
59. A. H. Reshak, Indian Institute of Technology-Rookee, Ph.D. thesis, India **(2005)**.
60. A. H. Reshak; Theoretical investigation of the electronic properties, and first and second harmonic generation for cadmium chalcogenide; *J. Chem. Phys.* 124, 014707 **(2006)**.
61. A. H. Reshak; Electronic, linear, and nonlinear optical properties of III–V indium compound semiconductors; *J. Chem. Phys.* 125, 034710 **(2006)**.
62. C. Ambrosch-Draxl and J. Sofo; Linear optical properties of solids within the full-potential linearized augmented planewave method; *Comp. Phys. Commun.* 175, 1 **(2006)**.
63. D. E. Aspnes; Energy-band theory of the second-order nonlinear optical susceptibility of crystals of zinc-blende symmetry; *Phys. Rev. B* 6, 4648 **(1972)**.
64. N. V. Smith; Photoelectron energy spectra and the band structures of the noble metals; *Phys. Rev. B* 3, 1862 **(1971)**.
65. A. H. Reshak, X. Chen, S. Auluck, and I. V. Kityk; X-ray diffraction and optical properties of a noncentrosymmetric borate $CaBiGaB_2O_7$; *J. Chem. Phys.* 129, 204111 **(2008)**.
66. A. H. Reshak, S. Auluck, and I. V. Kityk; Experimental and theoretical investigations of the first and second order optical susceptibilities of BiB_3O_6 single crystal; *Appl. Phys. A* 91, 451 **(2008)**; A. H. Reshak and S. Auluck; Band structure and optical response of 2H-MoX_2 compounds (X = S, Se, and Te); *Phy. Rev. B* 71, 155114 **(2005)**; and A. H. Reshak and S. Auluck; Full-potential calculations of the electronic and optical properties for 1T and 2H phases of TaS_2 and $TaSe_2$; *Physica B* 358,158 **(2005)**.
67. A. H. Reshak, I. V. Kityk, and S. Auluck; Investigation of the linear and nonlinear optical susceptibilities of $KTiOPO_4$ single crystals: Theory and experiment; *J. Phys. Chem. B* 114, 16705 **(2010)**.
68. A. H. Reshak; First-principle calculations of the linear and nonlinear optical response for GaX (X = As, Sb, P); *Eur. Phys. J. B* 47, 503 **(2005)**.
69. A. H. Reshak, S. Auluck, and I. V. Kityk; Optical susceptibilities of $Na_3La_9O_3(BO_3)_8$, ternary oxyborate nonlinear single crystal: Theory and experiment; *J. Phys.: Condens. Matter* 20,145209 **(2008)**.
70. A. H. Reshak, V. V. Atuchin, S. Auluck, and I. V. Kityk; First and second harmonic generation of the optical susceptibilities for the non-centro-symmetric orthorhombic $AgCd_2GaS_4$; *J. Phys.: Condens. Matter* 20, 325234 **(2008)**.
71. C. Casiraghi, A. Hartschuh, E. Lidorikis, H. Qian, H. Harutyunyan, T. Gokus, K. S. Novoselov, and A. C. Ferrari; Rayleigh imaging of graphene and graphene layers; *Nano Lett.* 7, 2711 **(2007)**.
72. R. R. Nair, P. Blake, A. N. Grigorenko, K. S. Novoselov, T. J. Booth, T. Stauber, N. M. R. Peres, and A. K. Geim1; Fine structure constant defines transparency of graphene; *Science* 320, 1308 **(2008)**.
73. Z. Sun, T. Hasan, F. Torrisi, D. Popa, G. Privitera, F. Wang, F. Bonaccorso, D. M. Basko, and A. C. Ferrari; Graphene mode-locked ultrafast laser. *ACS Nano* 4, 803 **(2010)**.
74. T. Gokus, R. R. Nair, A. Bonetti, M. Bohmler, A. Lombardo, K. S. Novoselov, A. K. Geim, A. C. Ferrari, and A. Hartschuh: Making graphene luminescent by oxygen plasma treatment; *ACS Nano* 3, 3963 **(2009)**.
75. J. F. Nye, Physical Properties of Crystals, Clarenndon, Oxford **(1967)**.
76. R. W. Boyd; Principles of Nonlinear Optics, Academic Press, NY **(1982)**, p. 420.

77. A. H. Reshak, S. Auluck, and I. V. Kityk; Linear and nonlinear optical susceptibilities for a novel borate oxide $BaBiBO_4$: Theory and experiment; *J. Solid State Chem.* 181, 789 **(2008)**.
78. A. H. Reshak, S. Auluck, D. Stys, I. V. Kityk, H. Kamarudin, J. Berdowski, and Z. Tylczynskif; Dispersion of linear and nonlinear optical susceptibilities for amino acid 2-aminopropanoic $CH_3CH(NH_2)COOH$ single crystals: Experimental and theoretical investigations; *J. Mater. Chem.* 21, 17219 **(2011)**.
79. A. H. Reshak, M. Piasecki, S. Auluck, I. V. Kityk, R. Khenata, B. Andriyevsky, C. Cobet, N. Esser, A. Majchrowski, M. Świrkowicz, R. Diduszko, and W. Szyrski; Effect of U on the electronic properties of neodymium gallate ($NdGaO_3$): Theoretical and experimental studies; *J. Phys. Chem. B* 113, 15237 **(2009)**.
80. R. W. Boyd, Nonlinear Optics, 3rd edn., Acadmic Press is an imprint of Elsevier **(2008)**, ISBN:978-0-12-369470-6.

Received: 4 August 2014. Revised/Accepted: 30 August 2014.